Oral presentation | Fluid-structure interaction
Fluid-structure interaction-I
Mon. Jul 15, 2024 10:45 AM - 12:45 PM Room A

[1-A-03] Numerical simulation of wave-structure interactions using a ghost-cell immersed boundary method

*D.C. Lo[1], R.S. Shih[2] (1. National Kaohsiung University of Science and Technology, 2. National Taiwan Ocean University)

Keywords: a ghost-cell immersed boundary method, body force function, absorbing wave layer function, wave-structure interactions, hydrodynamic force

Twelfth International Conference on Computational Fluid Dynamics (ICCFD12), Kobe, Japan, July 14-19, 2024

ICCFD12-2024-xxxx

Numerical simulation of wave-structure interactions using a ghost-cell immersed boundary method

D. C. Lo*, R. S. Shih**

*Corresponding author: loderg@nkust.edu.tw

* National Kaohsiung University of Science and Technology, Kaohsiung, Taiwan.

** National Taiwan Ocean University, Keelung, Taiwan

Abstract: A computational study of a viscous incompressible free-surface flows is developed for the wave-structure interaction problems using a ghost-cell immersed boundary method. The sources function of momentum equations includes the body force function and absorbing wave layer function. The body force function is used for the treatment of immersed boundaries, in which the wave absorbing layer can prevent absolutely the undesirable secondary wave reflections if the outflow boundary condition is concerned. The volume of fluid (VOF) method is employed to solve the interfacial values between the water and air phases, so that the surface elevation can be computed by solving the VOF equation. The numerical method based on the free-surface flow model is validated and extended to cover the wave-structure interactions cases for the wave propagation over a submerged bar, and a solitary wave over a various kinds of submerged breakwater. The efficiency of the proposed model is demonstrated to simulate the hydrodynamic force of wave acting on the structure by using an immersed boundary method.

Keywords: Free-surface flows, Ghost-cell immersed boundary method, Wave-structure interactions.

1 Introduction

Numerical wave tank has focused to extract a deeper insight into the wave-structure interactions involving the arbitrary wave condition and complex bottom topography. Available mathematical and numerical models that are adopted to simulate wave transformation around the submerged structures, such as the non-linear shallow water wave equation, the Boussinesq type models, the non-linear inviscid Laplace's equation and Navier-Stokes based models [1-3]. Among them the Navier-Stokes based models are well-known to overcome the shortcomings of nonlinear shallow-water or Boussinesq type and inviscid model, particular while dealing with overturning, dispersion and breaking of waves. The focus of the present simulation is to extract the wave generation by an inlet wave boundary condition and exploit the physical process of wave deformation between the wave-structure interactions. Exhaustive computations are accordingly performed based on 2D Navier-Stokes equations involving the proper sources function into the momentum equations, while taking into account different values of incident wave height and period.

The analysis of nonlinear wave with the interaction of submerged bodies and near surface transient flow perturbations is significant to several areas of breakwaters and offshore structures. Many analytical methods have been developed to solve traveling and standing wave [4] problems associated with incompressible and inviscid fluids as well as for the solution of linear and low order non-linear problems [5]. Furthermore, the phenomena of wave propagations in shallow water channel are the classical problems of flows with free-surface. Theoretical studies of periodic wave and solitary waves have attracted many investigators to provide a series of works [6-8]. Numerical methods that are used to simulate wave generations can be classified into three major categories, namely volume of fluid (VOF)-inflow method, internal wave generation method, a piston type wave maker. The above formulations have been thoroughly investigated by various researchers for free-surface flow problems using different numerical methods. The VOF-inflow method pioneered by Hirt and Nichols [9] and the VOF method is a simple and effective technique for treating the flows with a free-surface. In the wave generation in VOF-inflow method, the desire wave can be generated by using the free-surface elevation and the

velocity components obtained from analytical solution. Lin and Liu [10] established a numerical scheme for wave generation over a two-dimensional shoaling and breaking in the surf zone. An active wave generating-absorbing boundary condition using a VOF-inflow method with was reported in [11-12]. Notably, the present study employed free-surface flow model to generate the desired wave in the water tank. The second category of the numerical models for the wave generation is the so called internal wave generation method in which a mass source function of the continuity equation is introduced in the governing equations inside the computational domain [13]. Lin and Liu [13] derived the fluid is alternatively injected or sucked into source region in order to generate the desired wave. The single phase is considered in the above mention models. The third category is the piston-type or flap-type wave maker to generate various types of waves according to the wavemaker period, stroke and the still water depth. Notably, the undesirable secondary wave reflections should be carefully taken into the consideration. Dean and Dalrymple [14] presented the linear wavemaker theory. This branch has attracted many investigators to use piston-type wave maker to generate the desired wave. Anbarsooz et al. [15] used the piston-type and flap-type wave makers to generate linear and non-linear waves in intermediate and deep water cases.

The immersed boundary (IB) method was firstly pioneered by Peskin [16] using a structure grids with Cartesian coordinate system. The IB method has a simple way to tackle the flow problems with complex stationary or moving boundaries considerably. A series of works investigated on the numerical algorithms of IB method. In this study, the continuous forcing term is included in the Navier-Stokes equations prior to the discretization process. Notably, the properly imposition of boundary conditions at the immersed boundary is complicated by the Cartesian grid method. The IB method has a simple way to treat the immersed boundary through the underlying Cartesian mesh in an arbitrary manner. The treatment of immersed boundaries is a key issue to guarantee the accuracy and the conservation property of the underlying numerical solver. The combinations of IB and VOF methods are used to generate the desired wave for a series applications of wave-structure interactions, such as the wave deformation and decomposition during the processes of wave-structure interaction. The wave forces act on the submerged structure is computed utilizing on a computational fluid dynamics (CFD) with the consideration of a periodic waves and various types of submerged structures.

2 Mathematical Model

2.1 Free Surface Flow

Assuming the incompressibility for the fluid medium, the governing equations for free-surface flows with the wave absorbing layer and the immersed bodies can be expressed by means of the conversation of mass, conversation of momentum, the modeled 2D unsteady incompressible flow are as follows:

$$\nabla \cdot \mathbf{u} = \mathbf{0} \tag{1}$$

$$\frac{\partial \mathbf{u}}{\partial \mathrm{t}} + \nabla \mathbf{u}\mathbf{u} = -\nabla \mathrm{p} + \frac{\mu}{\rho}\nabla \cdot \left(\nabla \mathbf{u} + \nabla^{\mathrm{T}}\mathbf{u}\right) + \mathbf{g} + \mathbf{f} - \mathrm{A_b}\mathbf{u} \tag{2}$$

Here, the computational domain contains two different fluids with water and air, f denotes for immersed body forces, and A_b denotes the absorbing coefficient. g is the gravity acceleration vector, t is time The parameters describing the velocity vector in x and y directions, **u**, and pressure, P, are defined as the dimensional quantities in governing equations for physical interpretations once determined.

2.1 Wave Generation Boundary Conditions

2.1.1 A solitary wave boundary condition

The initial conditions for velocity and the free-surface height are specified in u=u(t); $h_s = h_s^0$ at t=0. As far as initial condition for the free-surface height and velocity are concerned, we adopt second order formulae for the free-surface profile and velocity as initial solitary wave.

$$h_s = h + \frac{H}{\cosh^2(\omega_\alpha)} - \frac{3}{4}\frac{H}{h}\frac{H}{\cosh^2(\omega_\alpha)}\left[1 - \frac{1}{\cosh^2(\omega_\alpha)}\right] \tag{3}$$

$$U = \sqrt{gh}\frac{H}{h}\left[1 + \frac{1}{4}\frac{H}{h} - \frac{3}{2}\frac{H}{h}(\frac{z}{h})^2\right]\sec h^2(\omega_\alpha) + \frac{H}{h}^2\left[-1 + \frac{9}{4}(\frac{z}{h})^2\right]\sec h^4(\omega_\alpha) \tag{4}$$

$$W=\sqrt{gh}\sqrt{3}(\frac{H}{h})^{3/2}\frac{z}{h}\sec h^2(\omega_\alpha)\cdot\tanh(\omega_\alpha)\left\{1-\frac{3}{8}\frac{H}{h}-\frac{1}{2}\frac{H}{h}(\frac{z}{h})^2+\frac{H}{h}\left[-2+\frac{3}{2}(\frac{z}{h})^2\right]\sec h^2(\omega_\alpha)\right\} \quad (5)$$

$$\omega_\alpha=\frac{(x-x_c)}{h}\sqrt{\frac{3}{4}\frac{H}{h}}(1-\frac{5}{8}\frac{H}{h}) \quad (6)$$

where h_s is the free-surface height, h is the initial depth of water, H is the wave height of a solitary wave, x_c is initial position of a solitary wave in the x-direction.

2.1.1 Periodic wave boundary condition

For the periodic wave, we adopt the second-order Stokes wave condition as initial wave condition as

$$h_s=h+\frac{H}{2}\cos(kx-\omega t)+\frac{\pi H^2}{8L}\frac{\cosh kh}{\sinh^3 kh}(2+\cosh 2kh)\cos 2(kx-\omega t) \quad (7)$$

$$U=\frac{H}{2}\frac{gT}{L}\frac{\cosh kz}{\cosh kh}\cos(kx-\omega t)+\frac{3}{4}(\frac{\pi H}{L})^2C\frac{\cosh 2kz}{\sinh^4 kh}\cos 2(kx-\omega t) \quad (8)$$

$$W=\frac{H}{2}\frac{gT}{L}\frac{\sinh kz}{\cosh kh}\sin(kx-\omega t)+\frac{3}{4}(\frac{\pi H}{L})^2C\frac{\sinh 2kz}{\sinh^4 kh}\sin 2(kx-\omega t) \quad (9)$$

where wave speed, C, is computed by $C=gT/(2\pi)\tanh(kh)$

2.2 Volume of Fluid Method

The conservation of the fluid phase for the arbitrary material fluid point is governed by the VOF function, $0\le \mathrm{F}(\mathrm{x},\mathrm{y},\mathrm{t})\le 1$, subject to the condition as:

$$\frac{\partial \mathrm{F}}{\partial \mathrm{t}}+U\frac{\partial \mathrm{F}}{\partial \mathrm{x}}+V\frac{\partial \mathrm{F}}{\partial \mathrm{y}}=0 \quad (10)$$

The upstream/downstream cells act as donor/acceptor is adopted by depending on the direction of local velocity.

where the free surface curvature is obtained in terms of,

$$k=-(\nabla\cdot\mathbf{n})=\frac{1}{|\boldsymbol{n}|}\left[\left(\frac{\mathbf{n}}{|\boldsymbol{n}|}\cdot\nabla\right)|\boldsymbol{n}|-(\nabla\cdot|\boldsymbol{n}|)\right]$$

and $\mathbf{n}=\nabla \mathrm{F}$ is the unit normal as $\mathbf{n}=\frac{\mathbf{n}}{|\boldsymbol{n}|}=\frac{\nabla \mathrm{F}}{|\nabla \mathrm{F}|}$

2.3 Numerical Formulation Based on Projection Method

The predicted velocity from time level n to n+1, we make use of the Adams-Bashforth scheme for the time integration of convective term, while an implicit second-order Crank-Nicolson method is used for diffusion term. We adopted a fractional step projection method [17] to solve the Navier-Stokes Eqs. (11-13) with a second-order accuracy to decouple the variables of velocity and pressure as following,

$$\frac{\mathbf{u}^*-\mathrm{u}^{\mathrm{n}-1}}{\Delta \mathrm{t}}=\frac{1}{2}(3\mathrm{C}^{\mathrm{n}-1}-\mathrm{C}^{\mathrm{n}-2})+\frac{1}{2}(\mathrm{D}^*+\mathrm{D}^{\mathrm{n}-1})-\frac{\nabla \mathrm{P}^{\mathrm{n}-1}}{\rho(\phi)}+\mathbf{f}_\alpha^{n-1}+\mathbf{f}^{\mathrm{n}} \quad (11)$$

$$\nabla\cdot\left(\frac{\nabla \mathrm{p}}{\rho(\phi)}\right)^n=\frac{1}{\Delta \mathrm{t}}\nabla\mathbf{u}^*+\nabla\cdot\left(\frac{\nabla \mathrm{p}}{\rho(\phi)}\right)^{n-1} \quad (12)$$

$$\mathbf{u}^{\mathrm{n}}=\mathbf{u}^*-\Delta \mathrm{t}(\frac{\nabla \mathrm{P}^{\mathrm{n}}}{\rho(\phi)}-\frac{\nabla \mathrm{P}^{\mathrm{n}-1}}{\rho(\phi)}) \quad (13)$$

where the superscripts n, n-1, n-2 denote time steps and n is the current step, $\Delta \mathrm{t}$ is the time interval. $\mathbf{u}^*$ represents intermediate velocity. C and D are convections terms and diffusion terms, respectively. The second-order Adams-Bashforth scheme is adopted for the discretization of convective term. The convection term is discretized by Forum scheme. A semi-implicit Crank-Nicolson method is employed for diffusion term. The procedure can eliminate the viscous stability constraint. $\mathbf{f}_\alpha$ represents the surface tension force, gravity and the wave absorbing force.

The immersed structure on its surrounding flow is modeled through a forcing term **f** included in the incompressible Navier-Stokes equations. The forcing term appeared in Eq. (11) can be adopted to compensate the differences between the intermediate velocities and the desired velocity at the ghost-cell forcing point. Since the intermediate velocity vector $\mathbf{u}^*$ is undetermined, the forcing term in Eq. (11) cannot be calculated explicitly. An iterative numerical procedure can be used for computing the intermediate velocity $\mathbf{u}^*$ and forcing term $\mathbf{f}^{\mathrm{n}}$. The forcing term $\mathbf{f}^{\mathrm{n}}$ is computed in each time step to guarantee that the velocity at boundary surface is consistent with ghost-cell velocity $\mathbf{u}_g$. We have

$$\mathbf{f}^{n} = \frac{\mathbf{u}_g - \mathbf{u}^{n-1}}{\Delta t} + \frac{1}{2}(3C^{n-1} - C^{n-2}) - \frac{1}{2}(D^{*} + D^{n-1}) + \frac{\nabla P^{n-1}}{\rho(\phi)} - \mathbf{f}_{\alpha}^{n-1} \quad (14)$$

Fig. 1 depicts the schematic of the points used to compute the ghost-cell velocity variable located at the computational domain. As shown by Fig. 1, the regular points are allocated inside the immersed cell with the number of points inside the solid phase of each cut cell accounted. The simplest 2D approach is to construct a quadrilateral region surrounding the interpolating point, minimizing the probability of numerical instability. For the 2D cases as shown in Fig. 1, here the case considers two kinds of situations to interpolate the image point $\mathbf{u}_p$. The ghost-cell velocity $\mathbf{u}_g$ is the ghost node, dark square points denote the nearest fluid nodes and boundary point. Here we present three condition to interpolate the velocity of image point. As shown in Fig. (a) the $\mathbf{u}_i$ can be interpolated using four fluid points. Fig. 1(b) includes four fluid points and one image boundary point. The index cell of the image point only has three fluid points and one boundary point we can use four points to interpolate the velocity of image point. The image velocity value can be computed as follows,

$$u_p = \sum_{i=1}^{ns} w_i^k u_i \quad (15)$$

Where w_i is the weight of grid point. ns is the total number of interpolating points as shown in Fig. 1. ns is the total number of selected interpolation points. The weight should satisfy the consistency condition in order to the total source velocity in going from the surrounding points to the image point. The weighting summation of kth marker point (image point) should be satisfied as follows,

$$\sum_{i=1}^{ns} w_i^k = 1 \quad (16)$$

When the value of image point is obtained then the value at ghost cell point can be extrapolated through the boundary, as shown in Fig. 1. Here the distance between ghost cell forcing point and solid boundary point are equal to the distance between image point and solid boundary point. The flow variable is evaluated at the extrapolation point by employing the interpolation scheme. The value at the ghost node can be computed by

$$u_g = 2u_\Gamma - u_p \quad (17)$$

In the successive time step, the velocity, forcing function and pressure components acquired from the previous time step are used as initial conditions to calculate the values for the new time step. The above solution procedure is repeated until the prescribed time step is reached. The present interpolation stencil schemes involving a simple distance weighting function are implemented for evaluation of velocity vector at the forcing point adjacent to the body surface.

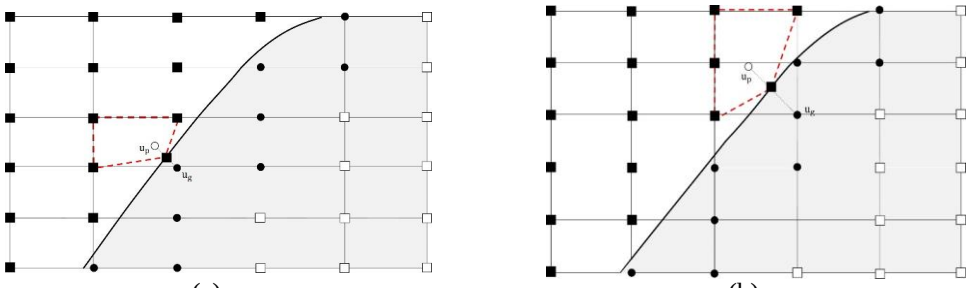

(a) (b)

Fig. 1. Schematic of the points used to compute the u_g-variable located at the computational domain. (●Ghost-cell forcing points; ○Interpolating points; ■ Fluid points; ▲ Solid points)

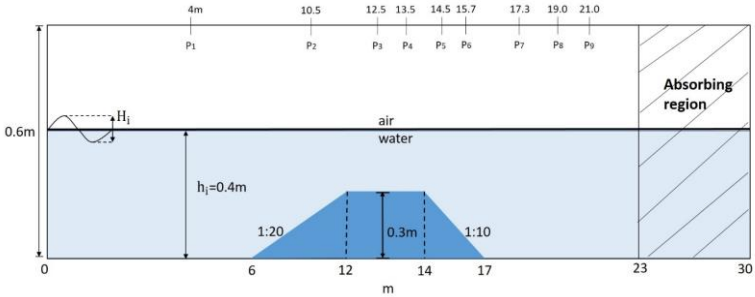

Fig. 2. Schematic of the computational domain for periodic wave pass over a trapezoid breakwater. (P1=4.0 m,P2=10.5 m,P3=12.5 m,P4=13.5 m,P5=14.5 m,P6=15.7 m,P7=17.3 m,P8=19 m,P9=21 m)

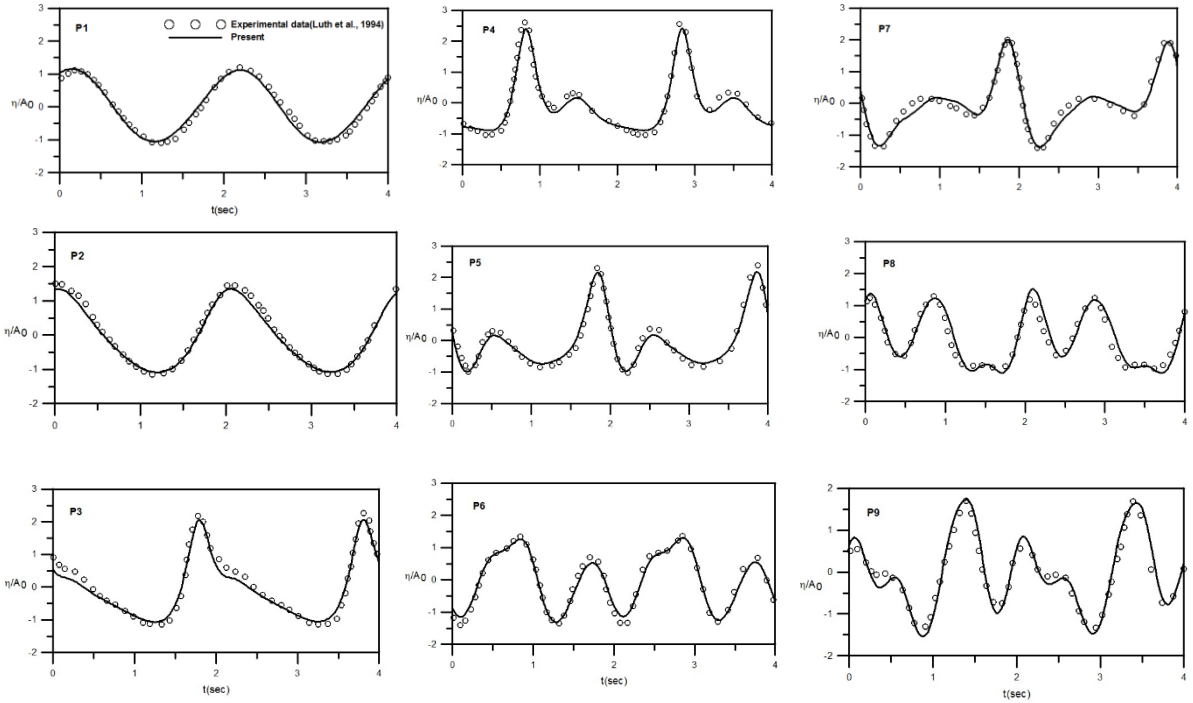

(a)

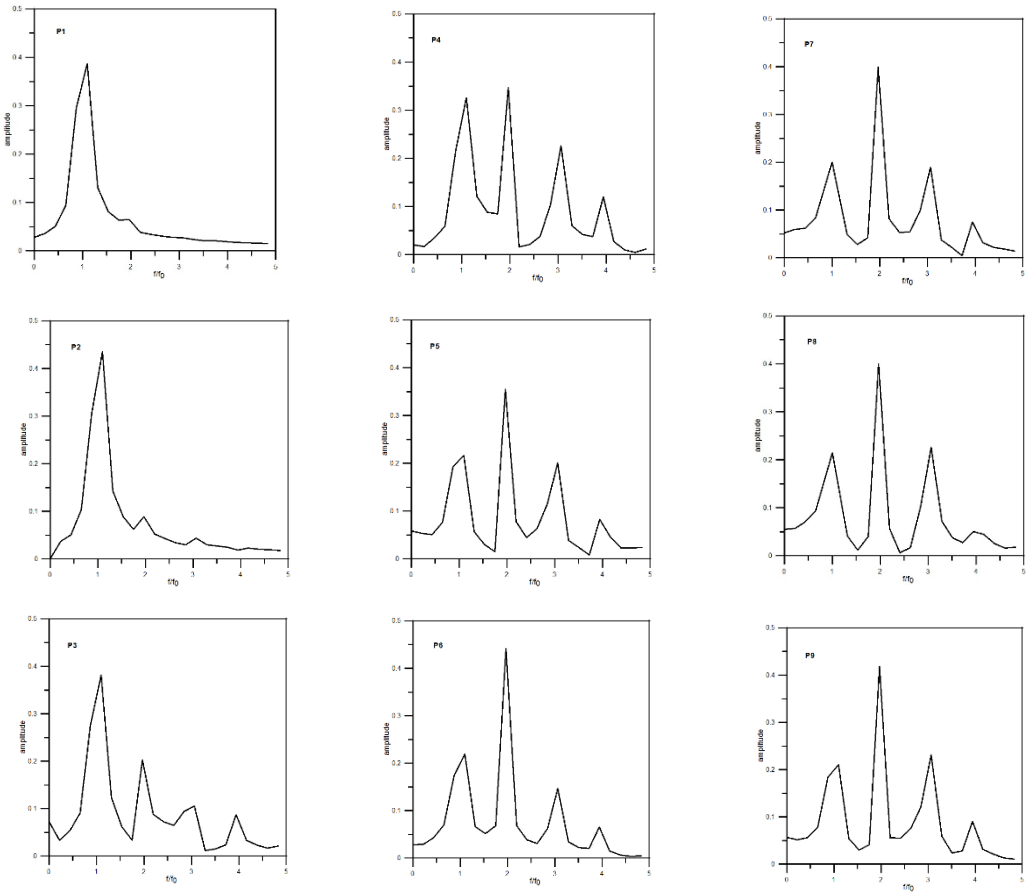

(b)

Fig. 3. Temporal free-surface undulation and its corresponding power spectra at nine different locations (H_i=0.02 m, T=2.02 s).

3 Results and Discussions

3.1 Wave Decomposition Process over a Trapezoid Breakwater

To examine the capability of the present free-surface flow model, we use the model to simulate the wave propagation over a submerged bar using an inlet wave boundary condition. The wave train propagating over a submerged bar, which has been experimentally by Luth et al. [18]. The experiment contains a flume with a length of 30 m and a water depth of 0.4 m as shown in Fig. 2. The bar is spread over stream wise length 11 m (between x = 6 and x = 17) and the top height of bar to be 0.3 m. Two angles of sloped beds are 1/20 and 1/10 slopes on the left and right side of a trapezoid breakwater. The present periodic wave generation was employed at beginning of x=0 m to a wave length wide, and the domain (23 m<x< 30 m) at right-hand side for the absorbing regions were added to the wave channel. An incident wave train with a wave height, H=2 cm, a wave period of T= 2.02 s was used for simulating the 2nd Stokes wave pass through a trapezoid breakwater, propagates from the left at x=0 m on the left-hand side, over the bar, to the beach at the downstream in their experimental setup only served for absorbing waves. There are several parts should be investigated in this study such as the comparisons of the free-surface elevation at the several measured locations. First, for the case of T=2.02 s was used as a test case with previous study in the literature. Fig. 3 exhibits the elevations of the nine numerical wave gauges. The six wave gauges were located at six different positions (P1=4.0 m, P2=10.5 m, P3=12.5 m, P4=13.5 m, P5=14.5 m, P6=15.7 m, P7=17.3 m, P8=19 m, P9=21 m). The results obtained of surface elevations at nine wave gauges are good agreement with the experimental results (Luth et al. 1994). The grid size with $\Delta x = 0.02$ m, $\Delta z = 0.005$ m was used to simulate the wave propagation over a bar. The phenomena of wave decomposition was vividly observed in several wave gauges. To better understand the developed near-interfacial dynamics, we now extract in Fig. 3 the detailed spectral behavior at various positions. Fig. 3 (a) and 3(b) show the temporal free-surface evolution and its corresponding power spectra at nine different locations. Notably, for the case of H=0.02 cm and T=2.02 s, the upstream sinusoidal-like flow undulations are primarily governed by the first mode (P1, P2, P3). However, the nonlinear free-surface distortion enhanced considerably behind the apex of the submerged structure (x≥ 12), the downstream interfacial nonlinearity (P4-P9) is practically driven by the second harmonic, the wave amplitude rise is quite significant at several locations of P4-P9.

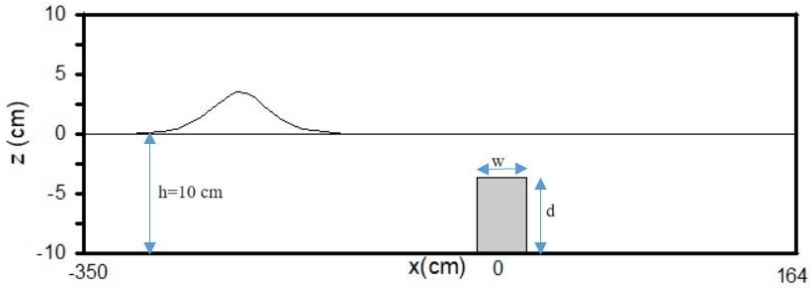

Fig. 4. Schematic of the computational domain for periodic wave propagating in the water channel (Unit: cm).

3.2 A solitary wave passing over different types of the submerged structures

A solitary wave propagates over a submerged bar, which has been experimentally by Li et al. [19]. The hydraulic model was conducted to analyze the formation and variations of eddies in fields generated by interactions of propagating solitary waves and various submerged BWs using PIV technique, and the hydraulic model experiment was performed in a two-dimensional small wave flume (length 5.0 m × width 8 cm × height 20 cm). A high frame rate (HFR) technique provided by Sony high-speed digital camera achieves a high frame rates of 960 fps at specific resolutions recorded the deformation of the waveform and wave-breaking effect to confirm the results measured by wave gauges, and the highest resolutions a picture frame support images with a resolution up to 1920 × 1080 pixels. The PivLab software presented by Thielicke and Stamhuis [20] was adopted to assist the eddy phenomenon and field distributions generated by the interactions of wave-structure.

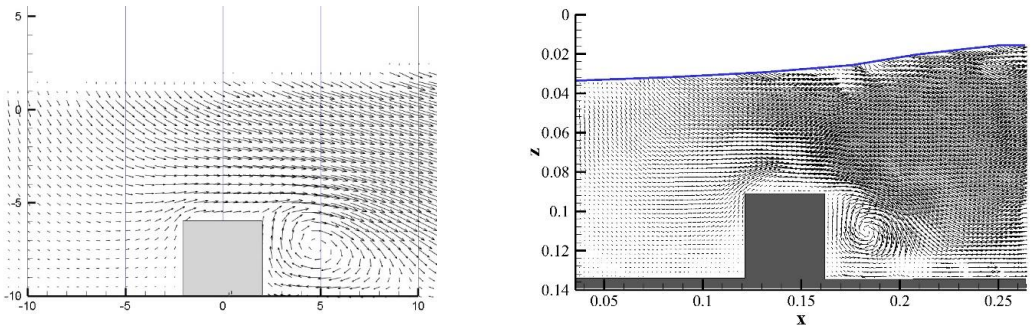

(a) d/h=0.4, w/h=0.4

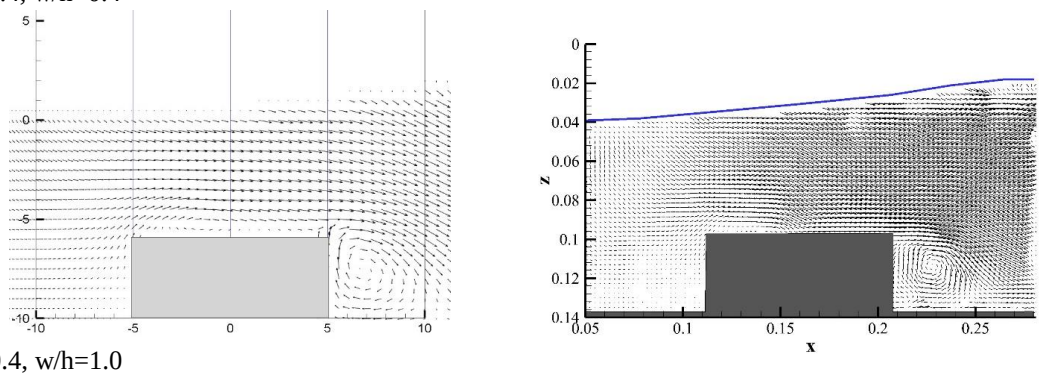

(b) d/h=0.4, w/h=1.0

Fig. 5. Vortex distribution around rectangular submerged structure. (Left: Numerical; Right: Experiment)

Initially, the Eqs. (3-6) is adopted to solve the elevation of free-surface and velocity distribution. The present numerical model is selected to test a solitary wave pass over a different types of submerged structure as shown in Fig. 4. The experiment contains a flume with a length of 5 m and a water depth of 0.1 m as shown in Fig. 4. The bar is spread over streamwise length w m (between x = -w and x = w) and the top height of bar to bed. To better understand the developed near-interfacial dynamics, we now extract in Fig. 5 the detailed vortex distribution around rectangular submerged structure between numerical and experimental study. Instantaneously velocity fields for a solitary wave with $H_i = 0.35$ m passing over different types of the submerged structures. For the case of triangular bar, the comparisons of numerical and experiment results for the velocity field as a solitary wave pass over triangular structure (d/h=0.4, w/d=2) at different times. Figs. 6-7 show the vortex distribution around triangular and rectangular submerged structure, respectively. For the numerical and experiment results, good accuracy is compared for different types of the submerged structures. In the triangular cases (Fig. 6), it shows the vortex development process of a solitary wave propagating over a triangular submerged obstacle when d/h = 0.4 and w/d=2, the vortex reaches its highest intensity when the wave peak passes over it, and the wave-induced vortex was found to be most powerful when the wave peak passes. when the solitary wave passes over the submerged triangular BW, a strong current on the levee surface caused by the falling water level impacts along the inclined slopping surface toward the water surface. As shown in the rectangular cases (Fig. 7), when the length of the submerged dike increases from w/h = 0.4 to 0.6, and to 1.0, the vortex occurs after the wave passes the BW, and where the wave surface drops as the wave crest is away, whereas the vortex occurs after the wave passes and the water surface away from the crest descends. Fig. 8 shows the results of the velocity field analysis using PIV of a vertical barrier BW. The waveform split-up as the solitary wave passes, part of the energy is blocked. The waveform variation is most obvious at d/h = 0.6, the location of the eddy current is approximately parallel to the top edge of the obstacle.

Determination of the drag and lift forces of surface waves acting on marine structures is important for the practical design of breakwaters. To comparison the impact force on different type on submerged structures, here we consider structure height/water depth (d/h) equal to 0.6. Fig. 9 shows the drag and lift forces of a solitary waves acting on a submerged structure. With the incident wave height of $H_i =$ 3.5 cm passing over the five types of submerged structures, the surface oscillation giving rise to the instantons water flow and hence the short variations of the drag and lift forces with respect to time as shown in Fig. 9. The absolute maximum drag and lift forces occurs for the cases of w=10 cm

(rectangular shape), and w= 10 cm (triangular shape), respectively. Analogous to the formation of the drag force, the wide length of rectangular shape also gives the largest drag force. Fig. 9(b) demonstrates that the triangular object (w=10 cm) causes the largest lift while the vertical structure contributes the smallest lift force. The minima drag and lift forces were found for the submerged structure of vertical shape. Notably, the drag and lift formed in the present circumstance is mainly due to the shapes of the submerged bars.

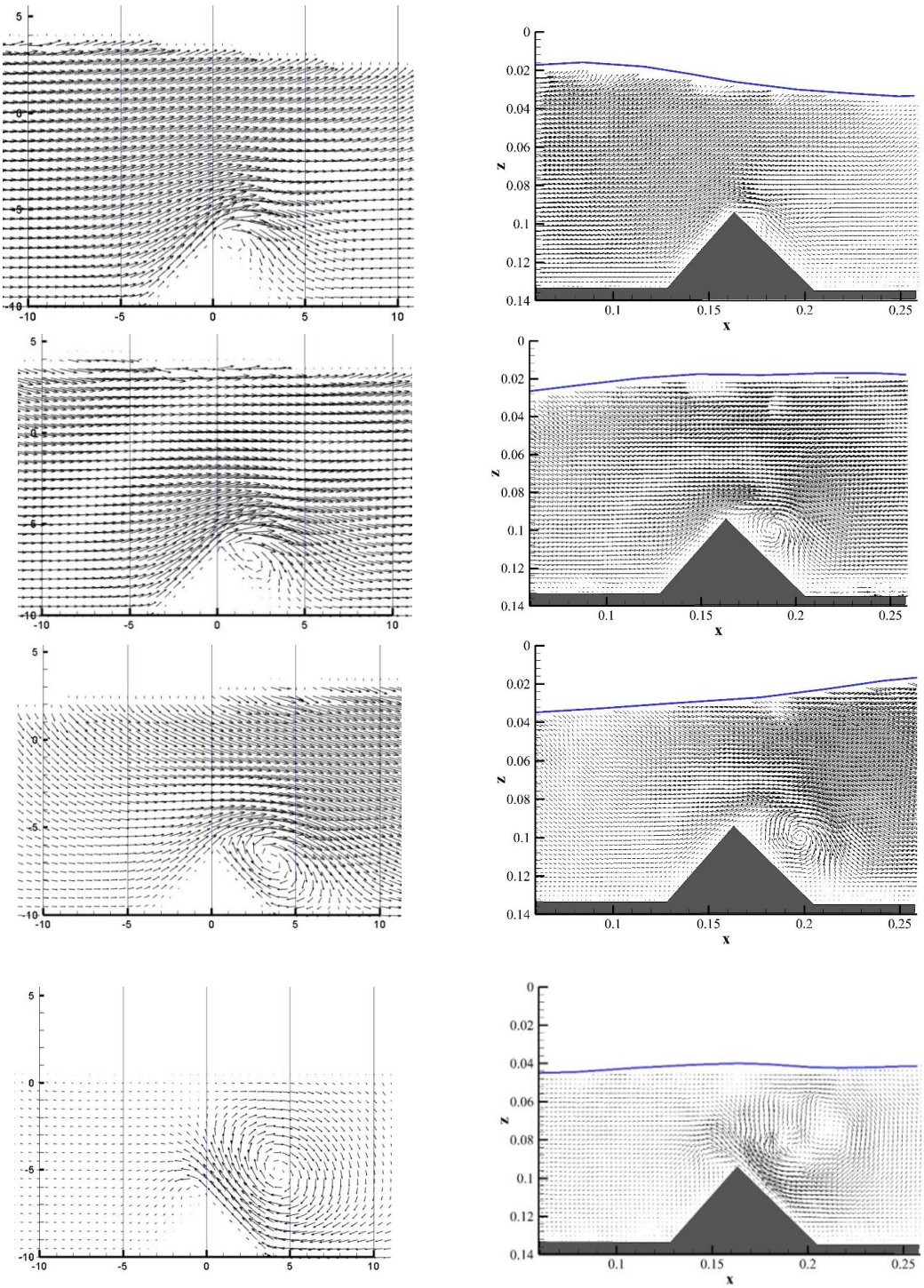

Fig. 6. Velocity field as solitary wave pass over triangular BW (d/h=0.4, w/d=2) at different times (Left: Numerical; Right: Experiment)

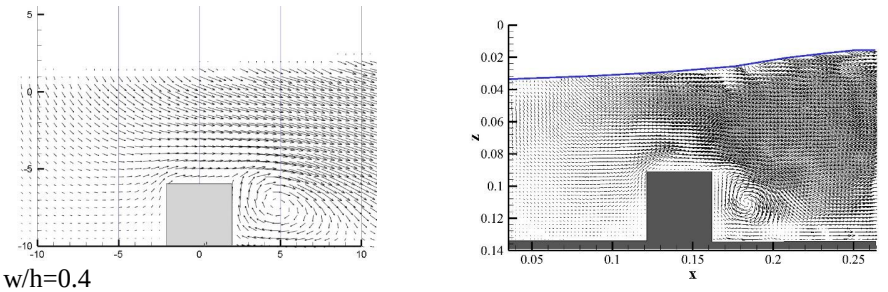

(a) d/h=0.4, w/h=0.4

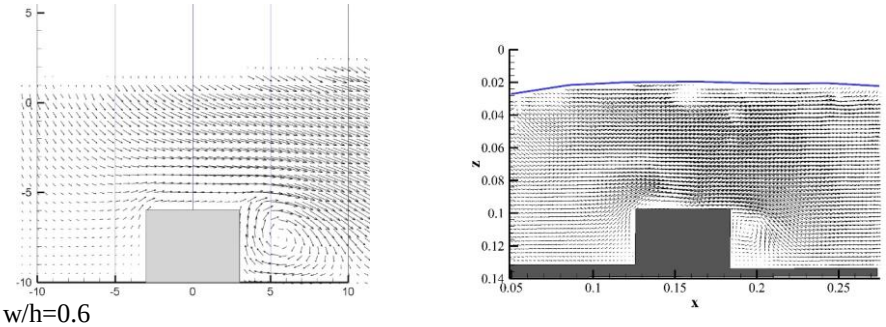

(b) d/h=0.4, w/h=0.6

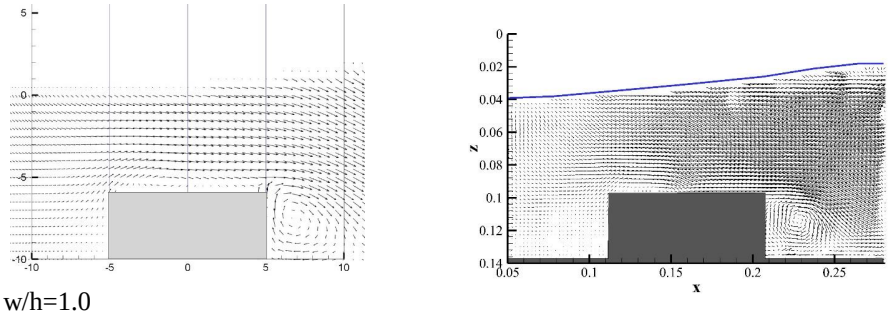

(c) d/h=0.4, w/h=1.0

Fig. 7. Vortex distribution around rectangular submerged BW. (Left: Numerical; Right: Experiment)

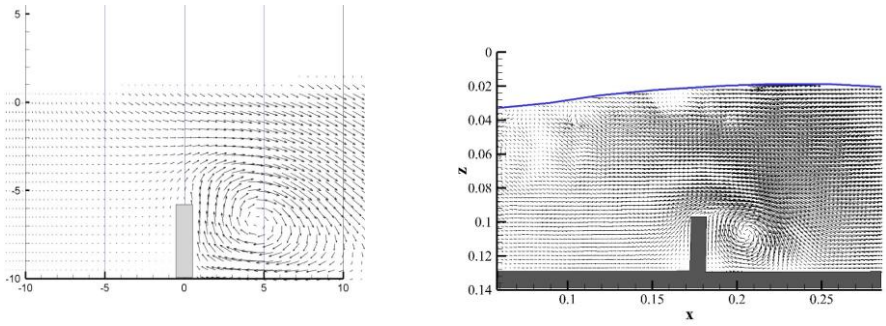

(a) d/h=0.4

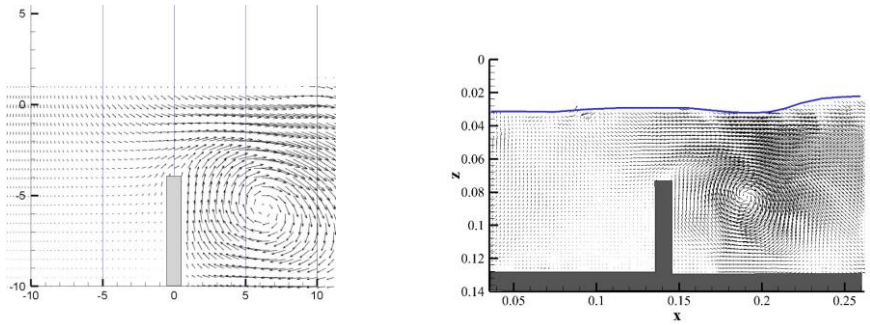

(b) d/h=0.6

Fig. 8. Solitary wave pass over vertical barriers at t=3 sec. (Left: Numerical; Right: Experiment)

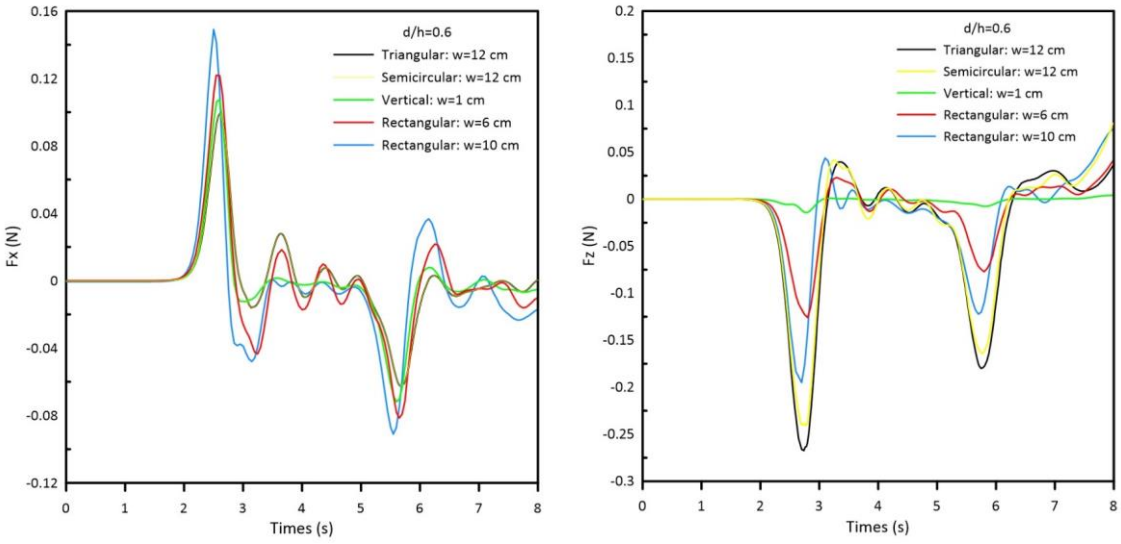

(a) (b)

Fig. 9. Comparisons of impact forces as solitary wave pass over a submerged structure(a) Drag force (b) Lift force.

4 Conclusion and Future Work

A computational study of a viscous incompressible free-surface flow model is developed for the wave-structure interaction problems. The sources function of momentum equation includes the body force function and absorbing wave layer function. The body force function is used for the treatment of immersed boundaries, in which the wave absorbing layer can prevent absolutely the undesirable secondary wave reflections. The VOF method is employed to solve the interfacial values between the water and air phases, so that the surface elevation can be computed by solving the VOF equation. The numerical method based on the free-surface flow model is validated and extended to cover the wave-structure interactions cases for (i) wave decomposition process over a trapezoid breakwater, (ii) interaction between a solitary wave and many different kinds of submerged structure in a viscous fluid. The efficiency of the free-surface flow model is demonstrated to simulate the hydrodynamic force of wave acting on the structure by using a ghost-cell immersed boundary method.

References

[1] R. Guanche, I. J. Losada, J. L. Lara. Numerical analysis of wave loads for coastal structure stability. Coast. Eng. 56: 543-558, 2009.

[2] J. L. Lara, I. J. Losada, R. Guanche. Wave interaction with low-mound breakwaters using a RANS model. Ocean Eng. 35: 1388-1400. 2008.

[3] I. J. Losada, J. L. Lara, R. Guanche, J. M. Gonzalez-Ondina. Numerical analysis of wave overtopping of rubble mound break waters. Coast. Eng. 31: 47-62. 2008.

[4] Newman, J. N. Marine hydrodynamics, MIT Press, Cambridge, MA. 1977.

[5] C. C. Mei. The applied dynamics of ocean surface waves, World Scientific. 1989.

[6] C. C. Mei. Radiation of solitons by slender bodies advancing in a shallow channel. J. Fluid Mech. 162: 53-67. 1983.

[7] P. Lin and P.L.F. Liu. Internal wave-maker for Navier-Stokes equations models. J. waterw. Port Coastal Ocean Eng. 125(4): 207-215. 1999.

[8] X. Liu, P. Lin, S. Shao. ISPH wave simulation by using an internal wave maker. Coast. Eng. 95: 160-170. 2015.

[9] C.W. Hirt and B.D. Nicholas. Volume of fluid method for the dynamics of free boundaries. J. Comput. Phys. 39: 201-225, 1981.

[10] P. Lin and P.L.F. Liu. A numerical study of breaking waves in the surf zone. J. Fluid Mech. 359: 239-264. 1998.
[11] B. Li and C. A. Fleming. Three-dimensional model of Navier-Stokes equations for water waves. J. waterw. Port Coastal Ocean Eng. 127 (1): 16-25. 2001.
[12] D. Apsley and W. Hu. CFD simulation of two- and three-dimensional free surface flow. Int. J. Numer. Method Fluid 42 (5): 465-491. 2003.
[13] P. Lin and P.L.F. Liu. Internal wave-maker for Navier-Stokes equations models. J. waterw. Port Coastal Ocean Eng. 125(4): 207-215. 1999.
[14] R. G. Dean and R. A. Dalrymple. Water wave mechanics for engineers and scientists. World Scientific Publishing Co. Re. ttd., Singapore. 1984.
[15] M. Anbarsooz, M. Passandideh-Fard, M. Moghiman. Fully nonlinear viscous wave generation in numerical wave tanks. Ocean Eng. 59, 73-85. 2013.
[16] C.S. Peskin. Flow patterns around heart valves: a numerical method. J.Comput. Phys. 10, 252-271. 1972.
[17] A. J. Chorin. A numerical method for solving incompressible viscous flow problem. J. Comput. Phys. 2: 12-26, 1967.
[18] H.R. Luth, G. Klopman, N. Kitou. Kinematics of waves breaking partially on an offshore bar. LDV measurements of waves with and without a net onshore current. Technical Report H-1573, Delft Hydraulics, Delft, The Netherlands, pp. 40, 1994.
[19] C.-Y., Li, R.-S. Shih, W.-K. Weng, T.-W. Liao. Analysis of vortex formation and energy dissipation during interaction of solitary-like waves with submerged breakwaters based on particle image velocimetry. Applied Ocean Res. 110: 102579, 2021.
[20] Thielicke, W. and Stamhuis, E. J., 2014, 'PIVlab - Time-Resolved Digital Particle Image Velocimetry Tool for MATLAB' (version: 2.31).